Available online at www.sciencedirect.com
ScienceDirect
Journal of Computational Physics 226 (2007) 89–103
JOURNAL OF COMPUTATIONAL PHYSICS
www.elsevier.com/locate/jcp

Numerical aspects of real-space approaches to strong-field electron dynamics

Astrid S. de Wijn [a], Stephan Kümmel [b,*], Manfred Lein [c]

[a] *Max-Planck-Institut für Physik komplexer Systeme, Nöthnitzer Strasse 38, D-01187 Dresden, Germany*
[b] *Physics Institute, University of Bayreuth, D-95440 Bayreuth, Germany*
[c] *Institut für Physik, Universität Kassel, D-34132 Kassel, Germany*

Received 13 April 2006; received in revised form 22 March 2007; accepted 28 March 2007
Available online 5 April 2007

Abstract

Numerical methods for calculating strong-field, nonperturbative electron dynamics are investigated. Two different quantum–mechanical approaches are discussed: the time-dependent Schrödinger equation and time-dependent density functional theory. We show that when solving the time-dependent Schrödinger equation, small errors in the initial ground-state wave function can be magnified considerably during propagation. A scheme is presented to efficiently obtain the ground state with high accuracy. We further demonstrate that the commonly-used absorbing boundary conditions can severely influence the results. The requirements on the boundary conditions are somewhat less stringent in effective single-particle approaches such as time-dependent density functional theory. We point out how results from accurate wave-function based calculations can be used to improve the density functional description of long-ranged, nonlinear electron dynamics. We present details of a method to reconstruct, numerically, the full, unapproximated, Kohn–Sham potential from the density and current of the exact system.

PACS: 31.15.Ew; 32.80.Rm; 34.80.Kw

Keywords: Time-dependent Schrödinger equation; Strong-field ionization; Density functional theory; Exchange-correlation potential; Real-space methods

1. Introduction

The rapid progress in laser technology over the past decade has opened up a new realm of experimental possibilities. The strengths of the electric fields that can be generated by pulsed lasers are comparable to the strength of the field that an atomic nucleus exerts on its electrons. At such field strengths, nonlinear and nonperturbative electron dynamics can be probed. This creates new possibilities in materials processing

* Corresponding author. Tel.: +49 (0) 921 55 3220.
E-mail address: stephan.kuemmel@uni-bayreuth.de (S. Kümmel).

0021-9991/$ - see front matter © 2007 Elsevier Inc. All rights reserved.
doi:10.1016/j.jcp.2007.03.022

and allows us to deepen our understanding of the fundamentals of light-matter interaction as well as to study electron correlation on a new, dynamical scale.

Situations in which both electron correlations and nonperturbative dynamics are important represent a great challenge to theory. Despite remarkable theoretical achievements [1–9], theory overall could not fully keep pace with the experimental advances. Whereas in ground-state electronic structure theory, *ab initio* or first-principles calculations are a standard and reliable tool to complement experimental investigations, the situation is different in the realm of strong-field excitations. Here, one frequently has to resort to simplified models instead of dealing with the full Hamiltonian. This is due to the much higher computational cost of fully time-dependent calculations. The strong, low frequency lasers typically used in experiments lead to large amplitude motion of the electrons which covers extended regions of space. Therefore, the techniques employing localized Gaussian- or Slater-type orbitals, which make many ground-state calculations feasible, cannot be used for describing the dynamics.

The numerical methods of choice for describing nonperturbative dynamics are grid-based real-space approaches. The discretization of the wave function or orbitals on a mesh allows for an unbiased representation so that the electronic density can spread to all regions of space and is not centered at certain pre-determined points as with localized basis sets. Furthermore, real-space methods allow for a flexible and straightforward treatment of boundary effects, e.g. via absorbing boundary conditions.

When one considers the physics of the problem of electrons in strong-fields, the most obvious and conceptually straightforward approach is to solve the time-dependent Schrödinger equation, e.g. by the above-mentioned real-space methods. When the time-dependent many-particle wave function has been determined, all observables can readily be computed from it. The disadvantage of this approach is that obtaining the correlated time-dependent wave-function in three-dimensional coordinate space is already a computationally overwhelming task for a two-electron system [9]. Even with further rapid advances in computer technology, it is unlikely that the dynamics of many-electron systems can be studied *ab initio* in the near and not-so-near future.

A completely different approach to quantum–mechanical dynamics is offered by time-dependent density functional theory (TDDFT) [10,11], which recasts the many-body problem into an effective single-particle picture (see Section 4.1). Since the fundamental variable in TDDFT is just the time-dependent density and since the calculation of the many-particle wave function is completely avoided, TDDFT can be computationally much more efficient than wave-function based quantum mechanics. It is one of the very few theories which have a chance to provide a first principles description of nonperturbative many-electron dynamics.

While TDDFT offers many possibilities, it has a serious drawback. Just like ground-state DFT, TDDFT, in principle, is an exact theory, but in practice, the exchange-correlation potential $v_{\mathrm{xc}}(\mathbf{r},t)$ which takes into account the many-body effects is not known exactly and must be approximated. The accuracy of TDDFT calculations depends sensitively on this approximation. Whereas "standard" approximations like the time-dependent local-density approximation (TDLDA) [10,12] work well for some tasks, like describing excitations in metal clusters [13–15], they dramatically fail for others [16]. In order to turn TDDFT into a reliable tool for calculating strong-field dynamics, improved approximations for the exchange-correlation potential must be developed. An important step towards this goal is revealing and understanding the fundamental properties of the exact $v_{\mathrm{xc}}(\mathbf{r},t)$.

The aim of this manuscript is to discuss numerical aspects and implications of both approaches to strong-field dynamics, i.e., wave-function theory and TDDFT. Furthermore, we show how results of highly accurate wave-function calculations can be used to develop a deeper understanding of TDDFT and the properties that good approximations for the unknown exact $v_{\mathrm{xc}}(\mathbf{r},t)$ must have. The manuscript is composed as follows: In Section 2 we briefly review TDDFT and the problem of correlated-electron dynamics in the Helium atom, and discuss the numerical model and tools we employ. In Section 3.1 we focus on how to calculate the time-dependent correlated wave function. We demonstrate that small errors in the ground state, from which the dynamics starts, can increase considerably during propagation of the wave function. An efficient scheme for calculating the ground state with high accuracy is presented. In Section 3.2 we discuss the influence of boundary conditions in wave-function-based calculations and in TDDFT. It is shown that the widely used absorbing boundary conditions must be handled with care and that this is in particular so when the correlated wave function is used. A method for obtaining insight into the correlation effects in TDDFT from results of

accurate wave function calculations by constructing the exact Kohn–Sham potential and pair-correlation function is discussed in Section 4. We finally offer conclusions in Section 5.

2. Concepts and problems

2.1. Time-dependent density functional theory

The fundamental idea of Kohn–Sham density functional theory is to map the real system of interacting electrons onto an auxiliary noninteracting system – the Kohn–Sham system – which yields the same density [10]. For an N-electron system, the density is constructed from auxiliary Kohn–Sham orbitals $\varphi_i(\mathbf{r},t)$ according to

$$n(\mathbf{r},t)=\sum_{i=1}^{N}|\varphi_i(\mathbf{r},t)|^2, \tag{1}$$

and the orbitals themselves are obtained as solutions of the Kohn–Sham equations,

$$\left[-\frac{\hbar^2}{2m}\nabla^2+v_s[n](\mathbf{r},t)\right]\varphi_j(\mathbf{r},t)=\mathrm{i}\hbar\frac{\partial}{\partial t}\varphi_j(\mathbf{r},t), \tag{2}$$

where m is the particle mass. In these effective single-particle equations, the Kohn–Sham potential v_s is chosen such that the noninteracting density equals the interacting one, and all observables can then (in principle) be calculated from the time-dependent density. The Kohn–Sham potential

$$v_s(\mathbf{r},t)=v_{\mathrm{ext}}(\mathbf{r},t)+v_h(\mathbf{r},t)+v_{\mathrm{xc}}(\mathbf{r},t) \tag{3}$$

consists of the external potential v_{ext}, the Hartree potential, which is equal to $v_h=e^2\int n(\mathbf{r}')/|\mathbf{r}-\mathbf{r}'|\,\mathrm{d}^3r'$ and the exchange-correlation potential v_{xc}. The latter is the crucial, nontrivial part of v_s that incorporates the many-body effects into the theory. An exact expression for this potential is not known, and it must therefore be approximated in practical TDDFT calculations.

2.2. Strong-field double ionization of the helium atom

Double ionization of the Helium atom in the strong field of a pulsed laser is one of the paradigm examples for strong-field phenomena. Instead of the sequential ionization that one would naively expect, i.e., the two electrons leave the nucleus independently, experiments [17] show a double ionization rate that is orders of magnitude larger than the rate expected from a sequential process. Intensive research, for example in references [3,18], clarified that the recollision mechanism [19] is responsible for the enhanced ionization with its famous "knee structure" [17]: an electron is first ionized and then accelerated back to the nucleus by the field of the laser. There it collides with the second electron and both leave the nucleus. A situation like the one just described must be treated nonperturbatively.

As discussed in Section 1, TDDFT is one of the very few approaches that offer a chance to calculate correlated, nonperturbative electron dynamics from first principles. Thus, it is a natural idea to employ TDDFT to study the question of enhanced double ionization. So far, however, all attempts in this direction have failed completely. Careful and detailed investigations [4,5,16] revealed that none of the functionals for $v_{\mathrm{xc}}(\mathbf{r},t)$ that are commonly employed in TDDFT calculations reproduces the characteristic knee shape in the intensity dependence of the double-ionization probability. Very recently, arguments have been put forward that offer an explanation for these failures [20,21,35].

Obtaining the double-ionization probability from a TDDFT calculation is a nontrivial task for two reasons. First, in order to obtain an accurate density, a good approximation for $v_{\mathrm{xc}}(\mathbf{r})$ is needed. Second, the density functional for the ionization probability is not known [16]. Both of these issues must be addressed in order to develop a reliable and accurate TDDFT description of ionization processes. In the following we discuss one method for investigating these issues.

It has recently been demonstrated that important properties of the time-dependent exchange-correlation potential can be extracted from accurate correlated wave-function calculations for a one-dimensional model of the Helium atom [20]. The essential idea in this approach is to extract the *exact* exchange-correlation potential from the exact time-dependent density by inverting the time-dependent Kohn–Sham equations.

The use of the one-dimensional atom is necessary, because of the extreme computational burden of non-perturbative calculations: as discussed in Section 3, very large grids are needed to capture the long-ranged dynamics that is associated with ionization. The use of this model is well justified for our purposes since a strong external electrical field forces the electrons to predominantly move one-dimensionally, namely in the direction of the field. The Hamiltonian for the one-dimensional Helium atom reads

$$H = \frac{p_1^2}{2m_e} + \frac{p_1^2}{2m_e} + V_e(r_1 - r_2) - 2V_e(r_1) - 2V_e(r_2) + V_f(r_1) + V_f(r_2), \tag{4}$$

where m_e is the electron mass. V_f is the potential due to the externally applied field, i.e., in our case a strong field that leads to an ionization process. $V_e(r)$ is the softened Coulomb potential,

$$V_e(r) = \frac{E_H}{\sqrt{x + (r/a_0)^2}}, \tag{5}$$

where E_H denotes the energy unit in Hartree atomic units, i.e., $E_H = 4.360 \times 10^{-18}$ J in SI units.

The softened Coulomb-interaction V_e with softening parameter x has been introduced above because the true, singular Coulomb-interaction cannot be used in one-dimensional calculations: the electrons could never pass the singularities. Since there is no unique way to fix the parameter x, one possible strategy would be to fit x to some experimental results. However, our investigations are concerned with fundamental effects that do not depend on the precise value of x and the results that we discuss in this manuscript do not depend qualitatively on the value of x. Consequently, we use the "canonical" value and set $x = 1$ [1].

The one-dimensional model has been extensively tested and it has been demonstrated that it captures the essential physics of the Helium double-ionization process [1,4–6]. Therefore, in all of the following discussions, we will consider the Hamiltonian in Eq. (4).

3. Computational methods

In the following we investigate the dynamics that result from Eq. (4) in two different ways. On the one hand, we consider the solution based on the time-dependent, correlated wave function. On the other hand, we look at the Kohn–Sham system with some approximation for v_{xc}. The initial state of the system is always the ground state, as the initial state of a system in an experiment is typically the ground state. The wave function is propagated using the split-operator method [24]. Derivatives are evaluated using Fourier transforms calculated with the fftw library [22]. A gridspacing of $0.25a_0$ and a time-step size of $0.025\hbar/E_H$ were used.

3.1. The influence of the initial state on strong-field dynamics

3.1.1. The importance of initial-state convergence

If a system exposed to a strong field is investigated numerically, then small errors can be magnified considerably during the numerical propagation in time. These problems can stem from errors in the initial state, or from errors introduced by insufficiently accurate propagation.

Calculating the ground state accurately can be tedious, but it is important for the following reason: an inaccuracy in the ground state means that contributions from excited states are present in the initial configuration. If an external field is applied, the exited states can be ionized more rapidly than the ground state. Thus, if the initial state has significant contributions from excited states, the dynamics will be dominated by these during the initial part of the simulation. Small errors in the ground state of the system may be amplified and/or significantly affect the results of calculations of some observables. As a consequence, the propagation must begin from a ground state which has been converged to such an accuracy that the dynamics which are of interest are not at any time overshadowed by the contributions from excited states.

To illustrate these remarks, two approximate ground-state densities are plotted in Fig. 1. One was found from the imaginary-time split-operator method with a timestep of $1\hbar/E_{\mathrm{H}}$. The other is from a much more accurate ground state. Both states were propagated in real time for $16\hbar/E_{\mathrm{H}}$ and $32\hbar/E_{\mathrm{H}}$ with the split-operator method, using a time-step of $0.025\hbar/E_{\mathrm{H}}$. The resulting densities after propagation are also shown in the figure. In the calculation that starts from the less accurate ground state, a small amount of density is ionized even though no field is applied. This is due to admixtures of excited states in the initial density. In a strong alternating field, such as we wish to investigate, this density might move through the atom repeatedly with high momentum. The error in the density may be amplified through the same recollision mechanism which causes the enhanced double ionization we are interested in. Thus, inaccuracies in the initial state may swamp out the effect we are looking for. Therefore, calculating the ground state accurately is very important and we will investigate this issue in greater detail in the following.

3.1.2. Obtaining the ground state by imaginary time propagation

Different ways can be followed in order to obtain the ground state accurately. One of the most straightforward ones is the direct numerical diagonalization of the Hamiltonian. However, for the very large grids needed for the description of long-ranged perturbative dynamics, this is not the most efficient method. Alternatively, the ground state may be found by evolving the system in imaginary time [23]. The imaginary-time propagation method is based on the evolution operator for a time step $-i\Delta t_\imath$, which works on the wave function according to

$$\psi(\mathbf{r}, -\mathrm{i}t - \mathrm{i}\Delta t_\imath) = \exp(-\Delta t_\imath H/\hbar)\psi(\mathbf{r}, -\mathrm{i}t). \tag{6}$$

We use the index $\imath$ to distinguish the time step $\Delta t_\imath$ in the imaginary-time propagation from the time step Δt in the real-time propagation. For long times, i.e., repeated application of this step, the wave function becomes dominated by the eigenfunction of H with the smallest eigenvalue, the ground-state eigenfunction.

The widely used split-operator method for calculating time evolution [24] may be applied to imaginary time as well. It requires two Fourier transforms per iteration and makes use of an approximation of the time-evolution operator which has errors of third order in $\Delta t_\imath$.

The error in the ground state and the ground-state energy produced in this scheme can be found from the eigenvalue equation,

$$\begin{aligned}\exp(-E_{\Delta t_\imath}\Delta t_\imath/\hbar)\phi_{\Delta t_\imath} &= \exp(-\Delta t_\imath T/(2\hbar))\exp(-\Delta t_\imath V/\hbar)\exp(-\Delta t_\imath T/(2\hbar))\phi_{\Delta t_\imath} \\ &= [\exp(-\Delta t_\imath H/\hbar) + \mathrm{O}(\Delta t_\imath^3)]\phi_{\Delta t_\imath}.\end{aligned} \tag{7}$$

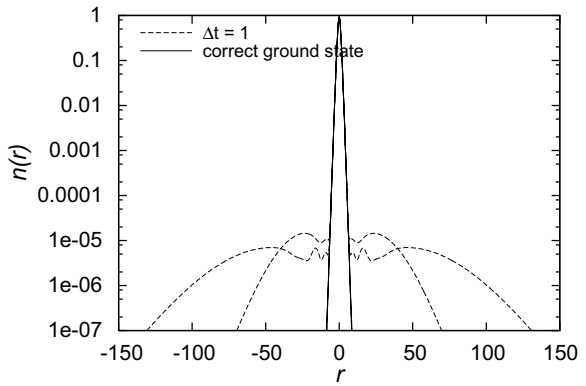

Fig. 1. Time evolution without external field for the fully converged ground state (full lines) and an approximate ground state from the imaginary-time method with time step $1\hbar/E_{\mathrm{H}}$ (dashed lines). Shown is the electron density at the three times $t = 0$, $t = 16\hbar/E_{\mathrm{H}}$ and $t = 32\hbar/E_{\mathrm{H}}$. Before the propagation, the two densities are indistinguishable on the scale of this plot. After propagation, the fully converged ground-state density appears unchanged, as it should be. However, the less accurate ground-state density spread out over the whole grid although no field was applied.

Here, $\phi_{\Delta t_\iota}$ and $E_{\Delta t_\iota}$ are the ground-state wave function and energy found from the imaginary-time scheme with a time step of Δt_ι and T and V denote kinetic and potential energy operators, respectively.

It is possible to expand $\phi_{\Delta t_\iota}$ and $E_{\Delta t_\iota}$ in Δt_ι,

$$\phi_{\Delta t_\iota} = \phi^{(0)}_{\Delta t_\iota} + \Delta t_\iota \phi^{(1)}_{\Delta t_\iota} + \Delta t_\iota^2 \phi^{(2)}_{\Delta t_\iota} + \mathrm{O}(\Delta t_\iota^3), \tag{8}$$

$$E_{\Delta t_\iota} = E^{(0)}_{\Delta t_\iota} + \Delta t_\iota E^{(1)}_{\Delta t_\iota} + \Delta t_\iota^2 E^{(2)}_{\Delta t_\iota} + \mathrm{O}(\Delta t_\iota^3). \tag{9}$$

Inserting these expansions into Eq. (7) and sorting orders in Δt_ι, one finds for the zeroth and first order terms

$$\phi^{(0)}_{\Delta t_\iota} = \phi^{(0)}_{\Delta t_\iota}, \tag{10}$$

$$-\frac{1}{\hbar} E^{(0)}_{\Delta t_\iota} \Delta t_\iota \phi^{(0)}_{\Delta t_\iota} + \Delta t_\iota \phi^{(1)}_{\Delta t_\iota} = -\frac{1}{\hbar} H \Delta t_\iota \phi^{(0)}_{\Delta t_\iota} + \Delta t_\iota \phi^{(1)}_{\Delta t_\iota}. \tag{11}$$

From Eq. (11) it follows that $H\phi^{(0)}_{\Delta t_\iota} = E^{(0)}_{\Delta t_\iota}\phi^{(0)}_{\Delta t_\iota}$, i.e., the zeroth order terms correspond to the exact values E and ϕ:

$$\phi^{(0)}_{\Delta t_\iota} = \phi, \tag{12}$$

$$E^{(0)}_{\Delta t_\iota} = E. \tag{13}$$

By substituting these results into the second order of Eq. (7) and dividing by $(\Delta t_\iota)^2$, one derives

$$E^{(1)}_{\Delta t_\iota}\phi + (E - H)\phi^{(1)}_{\Delta t_\iota} = 0. \tag{14}$$

By taking the innerproduct of this equation with the ground state and the excited states and making use of the fact that $\phi^{(1)}$ can be taken to be orthogonal to ϕ one can find the first-order errors. From the innerproduct with the ground state, one finds the linear error in the energy and from the innerproducts with excited states, one finds the linear error in the wave function:

$$E^{(1)}_{\Delta t_\iota} = 0, \tag{15}$$

$$\phi^{(1)}_{\Delta t_\iota} = 0. \tag{16}$$

By combining this with the third order of Eq. (7), one finally finds that

$$(E - H)\phi^{(2)}_{\Delta t_\iota} + [E^{(2)}_{\Delta t_\iota} + \mathrm{O}(1)]\phi = 0. \tag{17}$$

Once again making use of the fact that the errors in the wave function are orthogonal to ϕ and taking innerproducts, it is possible to derive that

$$E^{(2)}_{\Delta t_\iota} = \mathrm{O}(1), \tag{18}$$

$$\phi^{(2)}_{\Delta t_\iota} = \mathrm{O}(1)\phi. \tag{19}$$

Here the error in the energy is found from the innerproduct with the ground state and the error in the wave function is found from the innerproducts with the excited states. Eq. (18) shows that the error obtained in the ground-state energy with the imaginary-time split-operator propagation is of second order in the time step, although the error in the wave function due to propagation for one time step is of third order. The smallest possible relative error $\epsilon_{\Delta t_\iota}$ with which the ground state can be found in the imaginary-time scheme with split propagation operator, for small time-step size, is related to the time-step size by

$$\epsilon_{\Delta t_\iota} \sim \Delta t_\iota^2. \tag{20}$$

This is illustrated in Fig. 2.

Apart from the error due to the split-operator method, there is also an error in the ground state due to contributions from excited states that have not been fully damped out. This error can be defined as the relative contributions to the calculated ground state that are orthogonal to the ground state $\phi_{\Delta t_\iota}$ that would be found after infinitely many iterations with a time step Δt_ι. The rate of convergence, c, is the natural logarithm of the factor by which, after many iterations, the error in the state is reduced each iteration. Let the component of ψ that is orthogonal to the Δt_ι ground state be written as $\psi_\perp = \psi - \phi_{\Delta t_\iota}\langle\phi_{\Delta t_\iota}|\psi\rangle$. The rate of convergence is then defined as

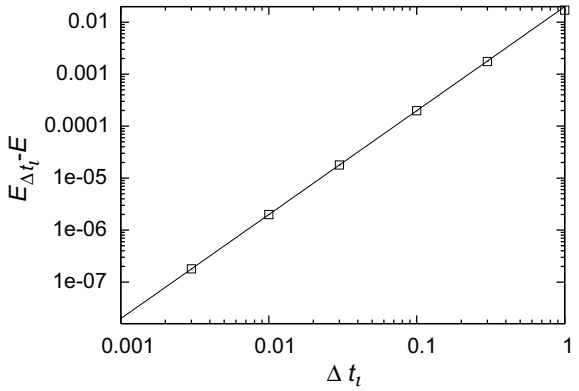

Fig. 2. The error in the ground-state energy obtained from the imaginary-time scheme as a function of time-step size. The ground-state energy is $-2.238E_{\mathrm{H}}$. The line is a fit and corresponds to $0.01985\Delta t_l^2$.

$$c = \ln\left[\left(\frac{\langle\psi_\perp(-\mathrm{i}t)|\psi_\perp(-\mathrm{i}t)\rangle}{\langle\psi(-\mathrm{i}t)|\psi(-\mathrm{i}t)\rangle}\right)^{\frac{1}{2}}\left(\frac{\langle\psi_\perp(-\mathrm{i}t-\mathrm{i}\Delta t_l)|\psi_\perp(-\mathrm{i}t-\mathrm{i}\Delta t_l)\rangle}{\langle\psi(-\mathrm{i}t-\mathrm{i}\Delta t_l)|\psi(-\mathrm{i}t-\mathrm{i}\Delta t_l)\rangle}\right)^{-\frac{1}{2}}\right]. \tag{21}$$

The rate of convergence can be calculated by writing the wave function which is propagated in imaginary time as a linear combination of the eigenstates that one would find with the split-operator method with time-step size Δt_l.

$$\psi(\mathbf{r}, -\mathrm{i}t) = \sum_j c_j(t)\phi_{\Delta t_l,j}(\mathbf{r}), \tag{22}$$

$$c_j(t) = c_j(0)\exp(-tE_{\Delta t_l,j}/\hbar), \tag{23}$$

where $E_{\Delta t_l,j}$ is the energy of the jth state and $\phi_{\Delta t_l,j}$ is the corresponding eigenfunction. Contributions from higher excited states will decrease faster than contributions from the first excited state and can be neglected for the calculation of the rate of convergence. The error in the ground state can then be written as

$$\left(\frac{\langle\psi_\perp(-\mathrm{i}t)|\psi_\perp(-\mathrm{i}t)\rangle}{\langle\psi(-\mathrm{i}t)|\psi(-\mathrm{i}t)\rangle}\right)^{\frac{1}{2}} = \frac{c_1(t)}{\sqrt{c_0(t)^2 + c_1(t)^2}}. \tag{24}$$

Except for the first few iterations, we have $c_1(t) \ll c_0(t)$, because $E_1 > E_0$. By substituting this in Eqs. (21) and (24), one finds

$$c = \ln\left\{\frac{c_0(t+\Delta t_l)c_1(t)}{c_0(t)c_1(t+\Delta t_l)}\left[1 + \mathrm{O}\left(\frac{c_1(t)^2}{c_0(t)^2}\right)\right]\right\} \approx \Delta t_l(E_1 - E_0). \tag{25}$$

If a highly accurate ground state is desired, denoted by a small relative deviation ϵ from the exact ground state, the time step must be small enough so that the smallest possible error $\epsilon_{\Delta t_l}$ from Eq. (20) does not exceed ϵ. This can be troublesome, as for a smaller error, a smaller time-step size is required, which leads to slower convergence by Eq. (25). By combining Eqs. (20) and (25), one may conclude from the rate of convergence that the number of required iterations M is

$$M \sim -\epsilon_{\Delta t_l}^{-1/2}\log\epsilon > -\epsilon^{-1/2}\log\epsilon. \tag{26}$$

3.1.3. A linear algorithm

Imaginary-time propagation is not the only method for finding the ground state. In principle, any operator which is strictly positive and strictly decreasing in the eigenvalues of the Hamiltonian will do. One may use an operator which meets these requirements and which can be implemented exactly, for example because it is a finite-order polynomial in H. This would remove the problem with the error dependence of the required num-

ber of iterations that exists in the imaginary-time split-operator scheme. In a fully exact system, however, such an operator cannot be constructed in any practical way. When the wave function is calculated on a grid, on the other hand, the system has a finite maximum energy (see below) and the eigenvalues of H are bounded from above.

On a grid with finite spacing Δx, the smallest representable wavelength is $\lambda_{\min} = 2\Delta x$, which corresponds to a maximum wave vector $2\pi/\lambda_{\min}$. Thus, the maximum momentum component in a specific direction for each electron is equal to $p_{\max} = \hbar\pi/\Delta x$. This sets an upper bound for the kinetic energy. If the potential energy is bounded from above by $U_{\max}$, an upper bound for the total energy is found from the sum of the two upper bounds,

$$E_{\max} = \frac{Nd\pi^2\hbar^2}{2m_e\Delta x^2} + U_{\max}, \tag{27}$$

where N is the total number of electrons and d is the number of dimensions. Hence, the operator $1 - H/E_{\max}$ is strictly positive and decreasing in the eigenvalues of H. It can be used to replace the time-evolution operator in Eq. (6) for finding the ground state. It is not used for this purpose very often, as the maximum energy becomes very large for fine grids [31]. It is, however, fully accurate, and, unlike the imaginary-time scheme, the practical implementation is not subject to an expansion in a time-step size. It also requires two Fourier transforms per iteration. The rate of convergence can be shown to be equal to

$$c = \ln\left(\frac{E_{\max} - E_0}{E_{\max} - E_1}\right). \tag{28}$$

For $E_{\max} \gg E_1$, this reduces to

$$c = \frac{E_1 - E_0}{E_{\max}}. \tag{29}$$

This is independent of the target error ϵ. Consequently, the number of iterations required to find the ground state within an error ϵ is proportional to $-\log\epsilon$.

3.1.4. Discussion and comparison

In general, wave functions exist which are left unaffected by the split operator with a finite time step. Of these wave functions, the one with the lowest energy could be considered to be the "ground state" of the split operator. The most reliable end result would be obtained if one could start from exactly this "ground state". One might think that the imaginary time-propagation operator with the same time-step size could produce this exact "ground state" of the real-time propagation operator. However, the imaginary-time propagation split operator makes a different error in the exact ground state of order Δt_i^2. The ground state found from the imaginary-time propagation is not mapped onto itself when propagated with the real-time-propagation operator with the same time-step size. Here the error is of order Δt^3, where Δt is the time-step size of the real-time propagation. At each time step a new error of order Δt^3 is introduced. Because the operator must be applied a number of times proportional to $1/\Delta t$ in order to cover a given interval in time, the error in the final wave function, compared to one from exact propagation of the same initial state, is of order Δt^2. The errors created by finite steps Δt and Δt_i have to be analysed independently of each other.

To decide which of the two methods described above is more efficient for finding the ground state, we substitute Eq. (20) into Eq. (25) and compare the result with Eq. (29). One concludes that the target accuracy for which the two methods are equally fast obeys the proportionality

$$\epsilon \sim \frac{1}{E_{\max}^2}. \tag{30}$$

The linear scheme speeds up the search for the ground state if the target error ϵ is small. In our experience, the most efficient way to find the ground state is to start by first converging roughly using imaginary-time propagation with a large time step, and then continuing with the linear scheme. Of course, it must be noted that any subsequent propagation must be done with a time-step size small enough not to introduce an error that would significantly outweigh the error due to the ground-state scheme. Finally, we note in passing that this scheme could also be used to accelerate the search for highly accurate excited states.

3.2. Absorbing boundary conditions

When a finite system is exposed to a strong, ionizing external electrical field, a significant fraction of the density may reach the boundary of the grid during the simulation. It is imperative to use boundary conditions which take care of this density without severely distorting the other properties of the system. Periodic boundary conditions are often out of the question for systems with strong fields since density may be accelerated indefinitely. Reflecting boundary conditions are also inadequate, as they reflect the density, which may be moving at high velocity, back towards the center of the system.

A common choice, which, as we will see, is a least of evils, is to use boundaries which absorb the density that reaches them. This can be implemented in several ways. In the split-operator context, the most convenient method is to add an imaginary term to the potential near the edge of the system in the time propagation [25]. In the following we will show that such boundary conditions may still affect the dynamics of the rest of the system.

The first and most obvious drawback of absorbing boundary conditions is that the dynamics at the boundary are irreversible. If the density oscillates back and forth, too tightly placed absorbing boundaries obviously can have a dramatic influence because they can remove density which in an exact treatment would return to the vicinity of the system in the next half cycle.

3.2.1. Single-particle orbital description

In methods based on single-particle orbitals, such as TDDFT or the Hartree–Fock method, the dynamics can be influenced by absorbing boundary conditions even in the case where density just moves away from the system (i.e. without rescattering). This is due to the fact that beyond the boundary there is no longer any density to interact with the density near the boundary. The behavior of the remaining density is modified compared to a system with boundaries that are further away. If the parts of the density that touch the boundaries are removed, the remaining density then "feels" the missing repulsion and is accelerated toward the boundary, where it, too, is removed.

An example of this effect in a realistic simulation is depicted in Fig. 3. It shows two snapshots of densities that result from Hartree–Fock calculations [26] of the one-dimensional model Helium atom which has been subjected to a static field that has been linearly ramped up. The field is cut off at a distance of $35a_0$ from the nucleus to prevent problems with strongly accelerated electrons. The boundary was implemented by adding an imaginary component to the potential, which is 0 everywhere except at the boundary, where it decreases from 0 to minus infinity as $4\ln(\cos((r-r_0)/20a_0))$, where r_0 is the position of the boundary. The full line

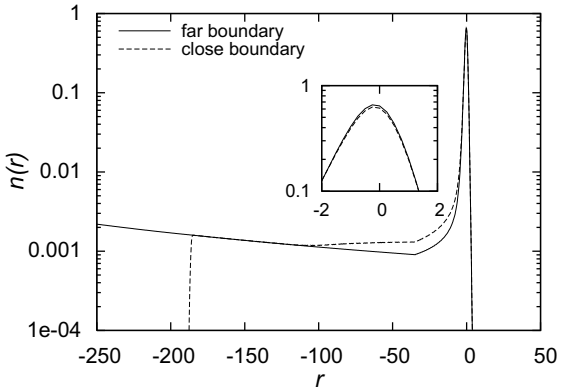

Fig. 3. Hartree–Fock results for the model atom in a static electric field that is linearly ramped up from field strength $0E_H/(ea_0)$ at $t = 0\hbar/E_H$ to a constant value of $0.141E_H/(ea_0)$, which is reached at $t = 12\hbar/E_H$. To prevent problems with strongly accelerated electrons, the field is cut off at $r = -35a_0$. The density is plotted as a function of the position after $t = 128\hbar/E_H$ for two different positions of the absorbing boundary, $-390a_0$ (full lines) and $-185a_0$ (dotted lines). With the nearby boundary, approximately 0.6 electron has been removed. The inset is an enlargement of the peak in the density near the nucleus. The average number of ejected electrons is about 0.54 for the calculation with the boundary further out and 0.58 with the closer boundary.

shows the density with an absorbing boundary at $390a_0$ after $128\hbar/E_H$ has elapsed. The dashed line shows the same situation with the absorbing boundary at $185a_0$, i.e., at a closer distance but at one which may naively still be considered "far away". Due to the Coulomb interaction, the density that is first to follow the field and move outwards repels the density that stays behind. In the system with the nearby boundary, some of the "first" density has been absorbed early and thus part of this interaction has disappeared. As a consequence, in the simulation in which the boundary is closer to the atom, the density moves into the boundary faster than it moves through a point at the same distance from the atom in a larger system. The errors introduced by this are noticeable even close to the atom, e.g. around $r = -20a_0$. The average number of ejected electrons is about 0.54 electron for the large system and 0.58 for the system with the closer boundary.

In the time-dependent Hartree–Fock or Kohn–Sham scheme, the observed effect can be viewed as a consequence of the particular structure of the equations. The electron–electron interaction appears in the equation in the form of a term that is nonlinear in the orbital so that a change in the orbital will also modify the effective potential. Therefore, the effect is, as our results show, rather large.

3.2.2. Correlated wave functions

In Kohn–Sham theory, the density by definition is obtained from Eq. (1) and the densities shown in Fig. 3 were calculated in this way. Eq. (1) follows from taking the expectation value of the number-density operator $\sum_{j=1}^{N}\delta(\mathbf{r}-\mathbf{r}_j)$ with a single Slater determinant, and there is nothing surprising about it. However, when absorbing boundary conditions are used, great care has to be taken in evaluating the density. In the following we illustrate this point by example of our model system.

In our Helium atom, the two electrons occupy the same spatial orbital $\varphi(\mathbf{r},t)$. Absorbing boundaries modify the orbital at the boundary only. Thus, when the density is computed from Eq. (1), $n(\mathbf{r},t) = 2|\varphi(\mathbf{r},t)|^2$, the direct effects of absorption on the density are restricted to the boundary region. Changes of the density in the inner region are possible only through the indirect effects discussed in Section 3.2.1.

However, let us carefully examine the process of calculating the density as the expectation value

$$\begin{aligned} n(\mathbf{r},t) &= \int \mathrm{d}^3 r_1 \int \mathrm{d}^3 r_2\, \varphi^*(\mathbf{r}_1,t)\varphi^*(\mathbf{r}_2,t) \sum_{j=1}^{2} \delta(\mathbf{r}-\mathbf{r}_j)\varphi(\mathbf{r}_1,t)\varphi(\mathbf{r}_2,t) \\ &= 2|\varphi(\mathbf{r},t)|^2 \int \varphi^*(\mathbf{r}',t)\varphi(\mathbf{r}',t)\,\mathrm{d}^3 r' \end{aligned} \tag{31}$$

in the presence of absorbing boundary conditions. When the orbital reaches the absorbing boundaries, the integral on the right-hand side of Eq. (31) will take a value of less than one. This has the consequence that the density at every point in space will be reduced by this factor, i.e., absorption at the boundary modifies the density not only at the boundary, but everywhere. Of course, this is a numerical artefact and for the case of the wavefunction being a single Slater determinant, one knows how to avoid it: By using Eq. (1) one implicitly sets the integral to the value 1 and, thus, can easily take into account that normalization should not have changed.

However, for a numerically calculated correlated wavefunction one cannot simply decompose the corresponding density into a sum over orbitals. Therefore, the above mentioned simple way of avoiding the just discussed numerical artefact caused by the absorbing boundaries cannot be used. One could avoid the problem by somehow taking into account in the normalization the part of the wavefunction which "has left the grid". Typically, however, this is not done and, therefore, one has to be prepared for unphysical effects as soon as density is absorbed at the boundary.

An example of this effect is shown in Fig. 4. In the correlated (quasi-exact) calculation in a static field the density near the nucleus is simultaneously reduced when density is removed at the boundary. By comparing the results shown in Fig. 3 to those of the correlated calculations shown in Fig. 4 one can see that the density remaining close to the nucleus is much more affected by the absorbing boundaries in the correlated calculation. The average number of ejected electrons in the correlated system is about 0.9 electron with the far away boundaries and 1.4 with the closer boundaries. In the uncorrelated calculations, with nearby boundaries the density at the nucleus is in better qualitative agreement with the results for the system with far-away boundaries.

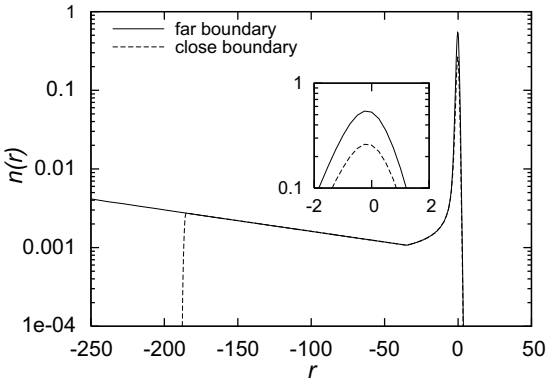

Fig. 4. Results for an exact, i.e., fully correlated calculation under the same conditions as in Fig. 3. With the nearby boundary, about 1.1 electron has been removed. In the inset the difference in the density near the nucleus is very clear. The average number of ejected electrons is about 0.9 electron with far-away boundaries and 1.4 with the closer boundaries.

This demonstrates that when interpreting calculations based on the correlated wave function, one has to keep in mind that absorbing boundary conditions can severely affect many observables even when relatively small amounts of density have been absorbed. Hence, absorbing boundaries must be used with great care in these cases.

4. New insight into the Kohn–Sham world

4.1. Reconstructing the Kohn–Sham potential

The propagation of correlated wave functions is time consuming and memory intensive. Moreover, as demonstrated above, the electron density calculated from a correlated wave function is very sensitive to absorbing boundaries. Computational approaches based on single-particle orbitals suffer much less from these problems. Yet, mean-field methods such as the Hartree–Fock method or the single-active-electron approximation clearly miss the effects that are of interest in correlated dynamics. Kohn–Sham density functional theory is very attractive since it has the potential to incorporate correlation effects into a framework that uses single-particle orbitals. However, as discussed in the introduction, better approximations for the exchange-correlation potential $v_{\mathrm{xc}}(\mathbf{r}, t)$ are needed before TDDFT will be a reliable tool for studying processes such as correlated double ionization. Most previous applications of TDDFT employed either the adiabatic local-density approximation or exchange-only potentials. Both of these methods are known to fail in predicting nonsequential double-ionization yields. A closer look reveals that not even single-ionization yields are predicted accurately by the exchange-only approach [7].

Little is known about exact properties of the full exchange-correlation potential. In this section we elaborate on a recently suggested way [20] how insight into the Kohn–Sham potential can be gained: the *exact* exchange-correlation potential is reconstructed from the quasi-exact time-dependent density. Similar techniques of reconstructing the Kohn–Sham potential were presented earlier by other workers [27,28], but not in the context of strong-field ionization. We note that even in the simplest correlated atom, the Helium atom, the calculation of the exact three-dimensional time-dependent density for an ionization process is currently out of reach due to the associated tremendous computational effort. The reconstruction of the Kohn–Sham potential is therefore restricted to model systems such as the one-dimensional Helium atom that we consider in this work. After having obtained the exact Kohn–Sham potential, it can be compared to existing approximations, so that deficiencies of these approximations are identified and information for the development of new exchange-correlation functionals can be inferred.

Our approach exploits the Runge–Gross theorem [29] which states that the Kohn–Sham potential is determined up to a purely time-dependent constant by the initial Kohn–Sham state and the time-dependent density. The initial Kohn–Sham state must be chosen such that it reproduces the initial density, as well as the first time

derivative of the density [30]. We consider here only two-electron systems starting from the ground state. We take the natural choice that the Kohn–Sham initial state consists of two electrons with opposite spins in the same spatial orbital. In this case, the two electrons will be described at all times by one orbital $\varphi(r,t)$. Working with only one orbital simplifies the calculation substantially, since the density is given simply by (one-dimensional notation is used in this section)

$$n(r,t) = 2|\varphi(r,t)|^2. \tag{32}$$

We take the density as given from the exact two-electron calculation so that we can immediately write

$$\varphi(r,t) = \left(\frac{n(r,t)}{2}\right)^{1/2} \mathrm{e}^{\mathrm{i}\alpha(r,t)}, \tag{33}$$

where the phase $\alpha(\mathbf{r},t)$ remains to be determined. The phase is related to the current in the Kohn–Sham system,

$$j_s(r,t) = \frac{\hbar}{m} n(r,t) \frac{\partial}{\partial r} \alpha(r,t). \tag{34}$$

By inserting the above ansatz for the orbital, Eq. (33), into Eq. (2), we find for the imaginary part of the Kohn–Sham potential

$$\mathrm{Im}\, v_s(r,t) = \frac{\hbar}{2n(r,t)} \left(\frac{\partial n}{\partial t} + \frac{\partial}{\partial r} j_s(r,t)\right). \tag{35}$$

The imaginary part must vanish, so the density and Kohn–Sham current must satisfy the continuity equation,

$$\frac{\partial n}{\partial t} + \frac{\partial}{\partial r} j_s(r,t) = 0. \tag{36}$$

The continuity equation holds also for the exact current $j(r,t)$ in the interacting system. Therefore, we have $\frac{\partial}{\partial r} j_s(r,t) = \frac{\partial}{\partial r} j(r,t)$. Taking into account that the currents must asymptotically go to zero for the case of the finite one-dimensional system considered here, it is thus obvious that the Kohn–Sham current must equal the current in the interacting system. We would like to recall that presently it is an open question whether this statement holds also in general three-dimensional systems. In the case considered here, we can replace in Eq. (34) the Kohn–Sham current by the true current, which allows to calculate the phase α from the exact density and current up to an arbitrary time-dependent constant,

$$\frac{\partial \alpha(r,t)}{\partial r} = \frac{m}{\hbar} \frac{j(r,t)}{n(r,t)}. \tag{37}$$

Knowing the phase, we construct the Kohn–Sham orbital, Eq. (33). From the time-dependent Kohn–Sham orbital we can calculate the Kohn–Sham potential. Naively, one might apply Eq. (2) and use a finite-difference method to calculate the time derivative. The momenta could be calculated by using a finite-difference method, or by using fourier transforms. However, since the split-operator method is used to propagate the two-electron wave function in time, a more consistent and numerically more stable way to obtain the Kohn–Sham potential is to invert the expression for the one-dimensional split-operator wave-function propagation,

$$\varphi(r,t+\Delta t) = \exp[-\mathrm{i}T\Delta t/(2\hbar)] \exp[-\mathrm{i}v_s(r,t+\Delta t/2)\Delta t/\hbar] \times \exp[-\mathrm{i}T\Delta t/(2\hbar)]\varphi(r,t). \tag{38}$$

From this one finds that

$$v_s(r,t+\Delta t/2) = -\frac{\hbar}{\Delta t} \arcsin \mathrm{Im}\left(\frac{\exp[\mathrm{i}T\Delta t/(2\hbar)]\varphi(r,t+\Delta t)}{\exp[-\mathrm{i}T\Delta t/(2\hbar)]\varphi(r,t)}\right) + k, \tag{39}$$

where k is an arbitrary constant which can be adjusted to impose a boundary condition on the potential. Typically, k is chosen to make v_s vanish at infinity.

A numerical problem arises in the calculation of α and v_s in the regions where the density is small, for example far from the nucleus. In those regions, the calculated two-electron density is not accurate and causes large

errors due to the denominators on the right-hand sides of Eqs. (37) and (39). For our present application, this is not a serious problem, as the density is always sufficiently large in the areas of interest.

4.2. The pair-correlation function

For the reasons mentioned in Section 2 we are interested in double-ionization probabilities. One issue with the calculation of multiple-ionization probabilities with TDDFT methods is the approximation of the ionization density functional. Although the Runge–Gross theorem tells us that, in principle, the multiple-ionization probabilities could be calculated exactly from the density, for practical purposes the exact functionals are not known and so must be approximated.

The ionization probabilities for no-, single- and double ionization, denoted by P_0, P_1 and P_2 respectively, can be expressed in the joint probability density $\rho(\mathbf{r}_1, \mathbf{r}_2, t)$ of two electrons. In an N-electron system the joint probability distribution can be found from the wave function through

$$\rho(\mathbf{r}_1, \mathbf{r}_2, t) = N(N-1)\left(\prod_{i=3}^{N} \int \mathrm{d}^3 r_i\right) \psi^*(\mathbf{r}_1, \mathbf{r}_2, \ldots, \mathbf{r}_N, t)\psi(\mathbf{r}_1, \mathbf{r}_2, \ldots, \mathbf{r}_N, t), \tag{40}$$

where the prefactor $N(N-1)$ is due to the fact that $\mathbf{r}_1$ and $\mathbf{r}_2$ may be the positions of any two electrons. In a two-electron system, this reduces to

$$\rho(\mathbf{r}_1, \mathbf{r}_2, t) = \psi^*(\mathbf{r}_1, \mathbf{r}_2, t)\psi(\mathbf{r}_1, \mathbf{r}_2, t) + \psi^*(\mathbf{r}_2, \mathbf{r}_1, t)\psi(\mathbf{r}_2, \mathbf{r}_1, t). \tag{41}$$

An electron can be considered ionized if it has left a subset A of R^d which surrounds the nucleus, e.g. in three-dimensional space a sphere with a radius of a few bohrs. The no-, single- and double-ionization probabilities can then be written as

$$P_0(t) = \frac{1}{2} \int_A \mathrm{d}^3 r_1 \int_A \mathrm{d}^3 r_2 \rho(\mathbf{r}_1, \mathbf{r}_2, t), \tag{42}$$

$$P_1(t) = \int_A \mathrm{d}^3 r_1 \int_{R^d \setminus A} \mathrm{d}^3 r_2 \, \rho(\mathbf{r}_1, \mathbf{r}_2, t), \tag{43}$$

$$P_2(t) = \frac{1}{2} \int_{R^d \setminus A} \mathrm{d}^3 r_1 \int_{R^d \setminus A} \mathrm{d}^3 r_2 \, \rho(\mathbf{r}_1, \mathbf{r}_2, t). \tag{44}$$

All correlation in the Kohn–Sham system is mediated through v_{xc}, and so the joint probability density cannot be extracted as easily as the single-particle density. It can be intuitively represented by the pair-correlation function [16]. The pair-correlation function is defined, in this context, as

$$g(\mathbf{r}_1, \mathbf{r}_2, t) = \frac{\rho(\mathbf{r}_1, \mathbf{r}_2, t)}{n(\mathbf{r}_1, t) n(\mathbf{r}_2, t)}. \tag{45}$$

In our singlet two-electron Hartree–Fock system, the pair-correlation function would be equal to 1/2 for all $\mathbf{r}_1$ and $\mathbf{r}_2$. The ionization-probability functionals can be directly related to the pair-correlation function.

So far, two approaches have been followed to calculate Helium ionization probabilities in TDDFT. The first is to simply evaluate the probabilities from the Kohn–Sham Slater determinant. This corresponds to using the Hartree–Fock value $g = 1/2$. The main advantage of this procedure is that it is simple. The main disadvantage is that is has been shown [5] that even with the exact density as input, these ionization probabilities differ noticeably from the exact ones. Consequently, attempts were made [16] to construct better functionals for the ionization probabilities by using approximate density functionals [32,33] for the pair-correlation function. Numerically, it was found [16] that using these functionals for g leads to ionization probabilities very similar to the ones obtained with $g = 1/2$. Here, we outline an argument why this is to be expected for a broad class of density functional models for g [34].

The above mentioned functionals for g are the sum of an exchange and a correlation contribution, i.e., $g(\mathbf{r}_1, \mathbf{r}_2) = g_x(\mathbf{r}_1, \mathbf{r}_2) + g_c(\mathbf{r}_1, \mathbf{r}_2)$. It is the correlation contribution that is of interest here. In the long-range limit, i.e., $|\mathbf{r}_1 - \mathbf{r}_2| \to \infty$, the correlation term $g_c(\mathbf{r}_1, \mathbf{r}_2)$ in the functionals that are derived from the homoge-

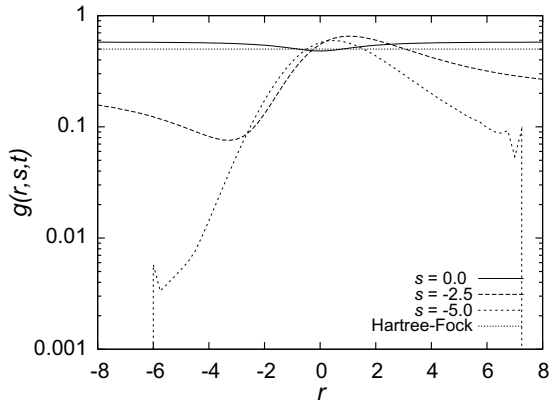

Fig. 5. Cross-sections of the pair-correlation function in the ground state for several positions of the reference electron. At $s = 5.0$ the joint probability density becomes so small that the edges can no longer be calculated accurately. For reference the pair-correlation function of a Hartree–Fock, which is equal to 1/2, independent of s and r, is also shown. The strange behavior for $s = 5.0$, around $\pm 6a_0$, is due to numerical inaccuracies related to the fact that the joint probability distribution and the density both become very small.

nous electron gas [32,33] goes to zero by construction. Now let us consider what this means for the single-ionization probability in the two-electron system, which according to Eqs. (43) and (45) is

$$P_1(t) = \int_A \mathrm{d}^3 r_1 \int_{R^d \setminus A} \mathrm{d}^3 r_2 \, n(\mathbf{r}_1) n(\mathbf{r}_2) g(\mathbf{r}_1, \mathbf{r}_2, t). \tag{46}$$

In this expression, $\mathbf{r}_1$ and $\mathbf{r}_2$ will be far apart from each other for the overwhelming part of the integral because $\mathbf{r}_1$ and $\mathbf{r}_2$ are to be taken from complementary regions of space. This means that the correlation contribution from the model functionals for g_c will be negligible. Thus, the result for P_1 will be very close to the exchange-only result. But from the relation

$$P_1 + 2P_2 = \int_{R^d \setminus A} \mathrm{d}^3 r_2 \, n(\mathbf{r}_2), \tag{47}$$

which can be verified by inserting Eqs. (43) and (44), it is clear that then, for given density, also P_2 will be very close to the exchange-only value. Due to the requirement $P_0 + P_1 + P_2 = 1$, the same statement then holds for P_0.

This shows that any functional $g_c[n](\mathbf{r}_1, \mathbf{r}_2)$ that tends to zero in the long-range limit will not lead to ionization probabilities that differ significantly from the exchange-only values. This is not a failure of the model functionals: They were designed to model the short-ranged (dynamical) correlation, whereas for the ionization problem, one is interested in long-range correlation effects.

Therefore, developing density functionals for the pair-correlation function from a new perspective is of great importance. As a tiny outlook we would here like to mention that in the one-dimensional model, the exact pair-correlation function can be calculated from the exact wave function, through Eqs. (41) and (45). In Fig. 5 several cross-sections of the pair-correlation function are shown for the correlated two-electron ground state of our model atom. When one electron is near the nucleus, the other electron is distributed almost according to the single-electron density, with only a relatively small hole near the nucleus. However, if the reference electron is further away from the nucleus, the hole in the distribution of the other electron is deeper and the electrons are more strongly correlated. Investigating the density functional of the pair-correlation function will be an important aspect of future work.

5. Conclusions

We investigated numerical problems that one has to face in calculating quantum mechanical, nonperturbative strong-field dynamics. Two different approaches to the quantum dynamics were discussed, namely propagation of the correlated many-particle wave function and time-dependent density functional theory. In both approaches, great care has to be taken to achieve an accurate initial state from which the dynamics is started. A method was proposed for achieving acceptable accuracy efficiently and with a straightforward algorithm

using a combination of imaginary-time propagation and a linear scheme. Another source of errors in dynamical calculations is the treatment of the boundaries. We discussed that absorbing boundaries can severely influence the results and that special care has to be taken in the interpretation of correlated wave-function calculations in which density has been absorbed at the boundaries. Finally, we pointed out how results from accurate wave-function based calculations can be used to improve the density functional description of long-ranged, nonlinear electron dynamics. We have shown how to reconstruct numerically the full, unapproximated Kohn–Sham potential from the density and current of the exact system. This scheme can be used to compare the exact exchange-correlation potential to commonly-used approximations.

Acknowledgments

S.K. acknowledges discussions with E.K.U. Gross, T. Kirchner, M. Mundt and financial support by the Deutsche Forschungsgemeinschaft.

References

[1] R. Grobe, J.H. Eberly, Phys. Rev. A 48 (1993) 4664.
[2] D.G. Lappas, A. Sanpera, J.B. Watson, K. Burnett, P.L. Knight, R. Grobe, J.H. Eberly, J. Phys. B 29 (1996) L619.
[3] A. Becker, F.H.M. Faisal, J. Phys. B 29 (1996) L197.
[4] D. Bauer, Phys. Rev. A 56 (1997) 3028.
[5] D.G. Lappas, R. van Leeuwen, J. Phys. B 31 (1998) L249.
[6] M. Lein, E.K.U. Gross, V. Engel, Phys. Rev. Lett. 85 (2000) 4707.
[7] N.E. Dahlen, R. van Leeuwen, Phys. Rev. A 64 (2001) 023405.
[8] X. Chu, S. Chu, Phys. Rev. A 64 (2001) 063404.
[9] J. Parker, K.T. Taylor, C.W. Clark, S. Blodgett-Ford, J. Phys. B 29 (1996) L33;
H.W. van der Hart, B.J.S. Doherty, J.S. Parker, K.T. Taylor, J. Phys. B 38 (2005) L207.
[10] E.K.U. Gross, J.F. Dobson, M. Petersilka, R.F. Nalewajski, in: R.F. Nalewajski (Ed.), Density Functional Theory II, Topics in Current Chemistry, vol. 181, Springer-Berlin, 1996, p. 81.
[11] C.A. Ullrich, S. Erhard, E.K.U. Gross, in: H.G. Muller, M.V. Fedorov (Eds.), Super Intense Laser Atom Physics IV, Nato ASI series 3/13, Kluwer, Dordrecht, 1996, p. 267.
[12] A. Zangwill, P. Soven, Phys. Rev. A 21 (1980) 1561.
[13] W. Ekardt, Phys. Rev. Lett. 52 (1984) 1925.
[14] P.-G. Reinhard, M. Brack, F. Calvayrac, C. Kohl, S. Kümmel, E. Suraud, C.A. Ullrich, Eur. Phys. J. D 9 (1999) 111.
[15] S. Kümmel, K. Andrae, P.-G. Reinhard, Appl. Phys. B 73 (2001) 293.
[16] M. Petersilka, E.K.U. Gross, Laser Phys. 9 (1999) 105.
[17] B. Walker et al., Phys. Rev. Lett. 73 (1994) 1227.
[18] R. Moshammer et al., Phys. Rev. Lett. 84 (2000) 447.
[19] P.B. Corkum, Phys. Rev. Lett. 71 (1993) 1994.
[20] M. Lein, S. Kümmel, Phys. Rev. Lett. 94 (2005) 143003.
[21] M. Mundt, S. Kümmel, Phys. Rev. Lett. 95 (2005) 203004.
[22] See http://www.fftw.org/.
[23] R. Kosloff, H. Tal-Ezer, Chem. Phys. Lett. 127 (1986) 223.
[24] M.D. Feit, J.A. Fleck Jr., A. Steiger, J. Comput. Phys. 47 (1982) 412;
R. Heather, H. Metiu, J. Chem. Phys. 86 (1987) 5009.
[25] A. Goldberg, B.W. Shore, J. Phys. B 11 (1978) 3339;
C. Leforestier, R.E. Wyatt, J. Chem. Phys. 78 (1983) 2334.
[26] For one-orbital systems, there is no difference between the Hartree–Fock definition of exchange and the Kohn–Sham definition of exchange.
[27] P. Hessler, J. Park, K. Burke, Phys. Rev. Lett. 82 (1999) 378;
P. Hessler, J. Park, K. Burke, Phys. Rev. Lett. 83 (1999) 5184;
P. Hessler, N.T. Maitra, K. Burke, J. Chem. Phys. 117 (2002) 72.
[28] I. D'Amico, G. Vignale, Phys. Rev. B 59 (1999) 7876.
[29] E. Runge, E.K.U. Gross, Phys. Rev. Lett. 52 (1984) 997.
[30] R. van Leeuwen, Phys. Rev. Lett. 82 (1999) 3863.
[31] For a related discussion see S. Kümmel, J. Comput. Phys. 201 (2004) 333.
[32] A.D. Becke, J. Chem. Phys. 88 (1988) 1053.
[33] J.P. Perdew, Y. Wang, Phys. Rev. B 46 (1992) 12947.
[34] We were made aware of this argument in a discussion with T. Kirchner.
[35] F. Wilken, D. Bauer, Phys. Rev. Lett. 97 (2006) 203001.